Polymer Chemistry

ROYAL SOCIETY OF CHEMISTRY

PAPER

View Article Online
View Journal | View Issue

Cite this: *Polym. Chem.*, 2025, **16**, 4040

Special interplay of hydrogen bonds and dynamic covalent bonds in sustainable polyurethane vitrimers with excellent recyclability and reprocessability

Xiaoyu Du,[a] Lang Shuai,[a] Shiqiang Wang,[a] Haitao Wu,[b] Jianglong Li,[a] Jianlong Wen,[a] Maiyong Zhu, *[a] Jie Hu*[a] and Yijing Nie *[a]

Constructing various reversible bond networks is one of the effective methods to endow polymers with high mechanical properties and recyclability. However, the interplay mechanisms between different reversible bond networks have not been fully understood. In the current work, polyurethane (PU) vitrimers containing covalent crosslinking networks, dynamic imine bond networks and hydrogen bond networks were prepared. The PU vitrimers exhibit high mechanical properties (tensile strength and modulus), excellent recyclability and reprocessability. The incorporation of the dynamic imine bonds leads to an increase of the number of hydrogen bonds in the PU vitrimers, and improves the degree of microphase separation between soft and hard segments. The presence of this unique interplay between the two different reversible bond networks endows the PU with superior comprehensive properties. These above findings are helpful in guiding the design and development of sustainable PU materials with high comprehensive properties.

Received 22nd July 2025,
Accepted 14th August 2025

DOI: 10.1039/d5py00728c

rsc.li/polymers

Introduction

At present, polymer materials are widely used in various aspects of people's lives, bringing them great convenience, but causing adverse effects on the environment.[1–3] Most synthetic polymer materials are difficult to completely degrade and will exist in the environment for a long time, causing environmental pollution and even human health problems.[4–6] Thus, the industry attaches great importance to the recycling of polymer materials. Generally speaking, thermoplastic linear polymer materials can be recycled, but it is difficult to recycle crosslinked thermosetting polymers.[7] Crosslinked thermosetting polymers are generally recovered through physical and mechanical crushing. However, this method requires a significant amount of energy consumption and can cause dust to float, resulting in environmental pollution. In addition, the mechanical properties of the polymers prepared by this recycling method are much lower than those obtained by normal production.

Therefore, finding ways to directly achieve effective recycling of thermosetting polymer materials (*i.e.*, a simple recycling method without significantly reducing the mechanical properties of recycled polymers) has always been a research hotspot in the field of polymer materials.[7,8] In theory, to achieve the recyclability or repeatability of crosslinked thermosetting polymers, some of the bonds or crosslinking points need to have dynamic reversibility (that is, the crosslinked thermosetting polymers need to contain dynamic reversible bonds, such as reversible covalent bonds or reversible non-covalent bonds).[9–11] Under the influence of external factors, such as the increase of temperature, dynamic reversible bonds will break and recombine, thus achieving the remoldability of crosslinked polymer materials. Inspired by the concept of dynamic combinatorial chemistry,[12–14] scientists have developed many polymer materials containing different reversible covalent bonds, such as imine bonds[15,16] and disulfide bonds,[17,18] undergoing Diels–Alder (D–A) reaction,[19] *etc*. These polymer materials containing reversible covalent bonds generally have recyclability, thus having great application prospects.[20,21] However, compared with ordinary covalent bonds, these reversible covalent bonds have lower bond energy, and thus the corresponding polymers containing the reversible covalent bonds exhibit poorer mechanical strength. In 2011, Leibler's group proposed the concept of vitrimers, which can maintain a constant crosslinking density.[22] But they can still flow when heated, and their viscosity depends on the kinetics of reversible dynamic exchange reactions.[22,23] The balance between mechanical properties and processability achieved by the vitrimers makes them highly promising in the

[a]*Institute of Polymer Materials, School of Materials Science and Engineering, Jiangsu University, Zhenjiang 212013, China. E-mail: maiyongzhu@ujs.edu.cn, 1000003080@ujs.edu.cn, nieyijing@ujs.edu.cn*
[b]*College of Polymer Science and Engineering, State Key Laboratory of Polymer Materials Engineering, Sichuan University, Chengdu 610065, China*

research of new crosslinked polymer materials that simultaneously achieve convenient recyclability and sufficient mechanical properties.

Various polyurethane (PU) vitrimers have been prepared by scientists.[24–28] For instance, Ji *et al.* prepared a PU elastomer containing dynamic diselenide bonds, which could be self-healed under visible light.[27] Xie *et al.* introduced as vanillin-derived Schiff base structure into PU chains, and the prepared PU can be recycled at high temperatures through the bond exchange of the amine bonds.[28]

In addition to dynamic covalent bonds, some other non-covalent bonds, such as hydrogen bonds[29–34] or coordination bonds,[35–37] have also attracted much attention from the academic community. Previously, our group prepared PU elastomers with high mechanical properties and high self-healing ability based on the construction of hydrogen bond networks by different methods, such as adding surface-modified nanoparticles,[38,39] introducing multiple hydrogen bond networks and flexible blocks onto PU chains,[40,41] constructing interpenetrating networks containing multiple hydrogen bond networks, flexible blocks, metal coordination and covalent crosslinking,[42] and blending polar rubber with PU elastomers.[43] Furthermore, various dynamic bonds are usually combined to enhance the overall performance of PU elastomers, such as strength, toughness and recyclability.[17,42,44,45] For PU materials, their molecular chains already contain groups that can form hydrogen bonds, such as urethane and carbonyl groups.[38–43,46] Therefore, after introducing dynamic covalent bonds into PU chains, a dual-network structure of hydrogen bonds and dynamic covalent bonds can be constructed. Unfortunately, most of the reports on PU vitrimers do not consider the interplay between hydrogen bonds and dynamic bonds. Dong's group prepared a new PU elastomer of high tensile strength based on the design of phase-locked dynamic bonds.[44] The disulfide bonds were introduced into hard segments, and then locked in hard microphase domains containing hydrogen bonds.[44] This indicates that the interplay between hydrogen bonds and dynamic covalent bonds indeed exists, and can directly affect the mechanical properties of PU materials.

Then, in the current work, we synthesized the PU vitrimers by the incorporation of dynamic aromatic imine bonds onto hard segments. In addition, molecular dynamics (MD) simulations were further performed to investigate the interplay between the hydrogen bonds and the dynamic covalent bonds. The prepared PU vitrimers exhibit excellent mechanical properties, recyclability and reprocessability. On one hand, the dynamic covalent bonds are locked in a hard microphase, and then they would exhibit significant stability during stretching, which is beneficial for the dramatic improvement in the mechanical properties. On the other hand, the presence of aromatic structures in the dynamic covalent bonds can also contribute to the enhancement in the mechanical strength. The simulation results revealed that the introduction of the dynamic imine bonds leads to an increase of the hydrogen bond number and the microphase separation degree.

Experimental section

Materials

Vanillin (Van), *m*-xylylenediamine, castor oil (CSO), isophorone diisocyanate (IPDI), and *N*,*N*-dimethylformamide (DMF) were purchased from Shanghai Macklin Biochemical Technology Co., Ltd. Dibutyltin dilaurate (DBTDL) and dichloromethane were purchased from Sinopharm Chemical Reagent Co., Ltd.

Synthesis of Van-OH

First, Van (7.6 g, 0.05 mol) was dissolved in 100 mL of dichloromethane, and then added into a three-mouth flask with a reflux device. Then, *m*-xylylenediamine (3.4 g, 0.025 mol) was dropped into the liquid mixture. After a yellow precipitate appeared, the mixture was heated to 45 °C and mechanically stirred for 6 h. After that, the yellow precipitate was collected and washed three times with dichloromethane. Finally, after vacuum drying at 45 °C for 24 h to a fixed weight, a yellow powdery substance was obtained, named Van-OH (9.867 g, yield of 89.7%, and melting point of 132–133 °C). The synthesis route of Van-OH is shown in Fig. S1(a).

Synthesis of PU vitrimers

Before synthesis, IPDI, Van-OH and CSO were first vacuum dried to remove excess moisture from the monomers to ensure accuracy in the experiments. For all the samples, the molar ratio of –NCO to –OH was fixed at 1.05 : 1. The CSO (9.33 g, 0.01 mol), Van-OH (1.616 g, 0.004 mol), DBTDL and DMF were added into the flask. Then, the mixture was stirred at 80 °C under a nitrogen atmosphere for 30 min to mix the reactants evenly. Subsequently, IPDI (4.65 g, 0.0209 mol) was added and stirred continuously at 80 °C for 3 h. The product in the flask was then poured into a Teflon mold, and the reaction occurred at 80 °C for 24 h. Finally, the system was heated to 150 °C for 8 h to obtain the PU vitrimer. The synthesis route of the PU vitrimer is shown in the lower part of Fig. S1(b). For simplicity, this PU vitrimer prepared using 0.004 mol Van-OH was named CVPU-1. As shown in Table S1, by changing the content of Van-OH, COPU (the PU without using the Van-OH), CVPU-2, CVPU-3, and CVPU-4 could be prepared following a similar synthesis route of CVPU-1 (the synthesis route of COPU is shown in the upper part of Fig. S1(b)).

Characterization

A Nicolet iS50 spectrometer from Thermo Fisher Scientific was used to collect Fourier transform infrared (FTIR) spectra. The total reflection infrared (ATR-IR) mode with a wavelength of 4000–600 cm^{-1} and a resolution of $\leq$0.09 cm^{-1} was selected. In addition, the temperature-dependent FTIR measurements were also conducted within a temperature range of 25 °C to 115 °C.

The ^{1}H-NMR and ^{13}C-NMR spectra of Van-OH were characterized using a Bruker's 400M type superconducting NMR spectrometer with dimethyl sulfoxide-D6 (DMSO-D6) as solvent.

The crosslinking density of PU vitrimers was measured using a VTMR20-010V-I low-field NMR analyzer from Newmark Analytical Instruments Co. The resonance frequency was 22 MHz, the magnet temperature was controlled at 35.00 ± 0.01 °C, and the probe coil diameter was 10 mm. The following equation was used for data fitting:

$$M(t) = A\exp\frac{-t}{T_{2A}} + B\exp\frac{-t}{T_{2B}} + A_0 \quad (1)$$

where $M(t)$ is the magnetisation intensity vector, A is the specific gravity of the crosslinked chains, B is the specific gravity of the dangling chains, A_0 is the fitting parameter, t is the test time, and T_{2A} and T_{2B} are the transverse relaxation times of the crosslinked and dangling chains, respectively. The crosslinking density (V_C) was calculated according to the following equation:

$$V_C = \frac{\rho}{2f\dfrac{\xi T_2^{av}}{aT_2^{rl}}C_\infty\dfrac{M_u}{n}} \quad (2)$$

where ρ is the sample density, T_2^{av} is the chemical and physical cross-linking parameter, which was obtained by software inversion fitting, f is the network cross-linking parameter, ξ is the conversion parameter, a is the rotational primary bond coefficient in the statistical chain segment, C_∞ is the proton spacing and local chain segment motion parameter, T_2^{rl} is the rigidity limit value, M_u is the average molecular mass, and n is the average number of primary bonds in the basic chain unit.

The mechanical properties of the films were tested at room temperature using a Shimadzu AGS-X universal testing machine from Japan. The sample size was a dumbbell-shaped strip of 2 × 35 mm, and the test rate was 10 mm min^{-1}. Each sample was tested three times in parallel, and the average value was reported. A cyclic tensile test was performed by stretching all the specimens to a fixed strain at a rate of 100 mm min^{-1} at 100% of the fixed strain and then unloading them to the initial state at the same rate and repeating the test 5 times. The dissipated energy was calculated as the area enclosed by the loading–unloading curve.

Dynamic mechanical analysis (DMA) of PU samples was conducted using the DMA242 E-type instrument from NETZSCH, Germany. The testing mode was tensile mode, and the temperature range was from −30 °C to 150 °C with an amplitude of 5 μm at a testing frequency of 10 Hz and a heating rate of 5 K min^{-1}. In addition, all samples were cut into rectangular strips of 12 mm × 5 mm × 1 mm. Thermomechanical analysis (TMA) was also performed using the DMA242 E-type instrument. By applying a 0.001 N pretension force to PU samples using a fixture, volume expansion curves of PU samples were tested from 50 °C to 250 °C under 5 kPa constant stress and a heating rate of 3 K min^{-1}.

The phase composition of PU samples was analyzed using a multifunctional X-ray diffractometer (XRD SmartLab) with an X-ray emission power of 9 kW in the range of 10° to 60°.

Small angle X-ray scattering (SAXS) measurement was used to test the degree of microphase separation of PU samples using an Anton Paar SAXSess MC2 instrument. The detector was a copper-targeted phototube with a tube voltage of 40 kV, a tube current of 40 mA, and a wavelength of 0.1542 nm.

Atomic force microscopy (AFM) measurements were performed at room temperature using a Bruker Dimenson ICON instrument, USA, with a pixel resolution of 256 × 256 and a randomly selected 1 μm × 1 μm surface.

The heat resistance of PU samples was tested using an STA449F3 comprehensive thermal analyzer from NETZSCH, Germany. The testing atmosphere was N_2, the starting temperature was room temperature, the ending temperature was 600 °C, and the heating rate was 10 °C min^{-1}.

The stress relaxation of PU samples was studied using a flat rheometer (HAAKE MARS 60). PU samples were placed on a plate, balanced at a preset temperature for 5 min, and then tested by applying 1% deformation.

The water contact angle (CA) was measured with deionized water at room temperature using a drop shape analyzer (KRUSS DSA100, Germany). The volume of water was 5 μL per drop, and the tests were repeated at 5 points for each sample, with each point tested for 30 s.

The CVPU films were cut into rectangles (25 mm × 12.5 mm × 0.3 mm) and placed between two identical iron blocks (100 mm × 25 mm × 2 mm) with an overlap area of 25 mm × 12.5 mm. The iron blocks with the films were subsequently placed in an oven at 180 °C for 30 min, and were then cooled to room temperature. The lap shear test was performed using the Shimadzu AGS-X universal testing machine at room temperature. For the reusability test of the CVPU films, the iron blocks that separated after the first overlap shear test were bonded again using the CVPU used the last time under the same conditions as the first bonding. According to the above procedure, the lap shear test was carried out again on the re-bonded iron blocks with the CVPU films.

Simulation details

The purpose of the current molecular simulations is to illustrate the influence of the incorporation of the dynamic bonds on hydrogen bond formation and microphase separation. To be specific, the types and quantities of hydrogen bonds were calculated to reflect the formation of hydrogen bonds, and the Flory–Huggins parameters for the interaction between hard and soft segments (χ_{mix}) were calculated to reveal the degree of microphase separation. As shown in Fig. S2, we constructed two model systems (the simulated CVPU system and the simulated COPU system) by referring to the molecular chain structures of two kinds of PU synthesized in the experiments (CVPU and COPU). Then, the systems were annealed under the NVT ensemble with T = 300 K–800 K, and the lowest energy conformation was obtained. Subsequently, the systems were relaxed for 500 ps under the NVT ensemble and the NPT ensemble successively, with a time step of 0.5 fs. The pressure was controlled by the Berendsen thermostat (0.1 MPa), and the temperature was controlled by the Anderson thermostat (298 K), and the COMPASS force field was selected for the simulations.[47]

Results and discussion

Design for material structures

The CVPU samples contain a triple network structure, including the network of the covalent crosslinking due to the introduction of the CSO chain segments onto the PU chains, the network of the hydrogen bonds, and the network of the dynamic covalent bonds due to the introduction of the imine bonds on the PU chains, as shown in the left panel of Fig. 1. The right panel of Fig. 1 also displays the detailed hydrogen bonds that can form in the CVPU samples. Mainly three types of hydrogen bonds can exist in the CVPU samples: the hydrogen bonds forming between the amine groups and the carbonyl groups both in the urethane groups, the hydrogen bonds forming between the amine groups in the urethane groups and the carbonyl groups in the CSO segments, and the hydrogen bonds forming between the amine groups in the urethane groups and the nitrogen atoms in the imine bonds.

Microphase separation between soft segments and hard segments can occur in the CVPU samples. The isocyanate segments and the Van-OH segments containing strong hydrogen bonding interactions and rigid structures act as hard domains, while the CSO segments act as soft domains. Under these conditions, there are also two other structural features associated with the imine bonds incorporated into the hard domains. First, as shown in Fig. S1(b) and Fig. 1, the dynamic imine bonds are located between two isocyanate segments, indicating that the dynamic covalent bonds are locked in the hard domains. This structural design idea is consistent with the concept of "phase-locked" dynamic bonds proposed by Dong's group.[44] Second, the Van-OH segments contain both the dynamic imine bonds and the rigid structures (benzenes).

Microstructures of PU vitrimers

Fig. S3(a) shows the FTIR spectrum of Van-OH. It can be seen that an absorption peak appears at 1639 cm^{-1}, corresponding to the stretching vibration of the C=N bonds.[16] In addition, there is no absorption peak at 1680 cm^{-1}, corresponding to the stretching vibration of the aromatic aldehyde.[48] These above results indicate the successful synthesis of the imine bonds. Furthermore, as shown in Fig. S3(b) and S3(c), peaks appear at 8.35 ppm and 162.23 ppm in the ^{1}H NMR and ^{13}C NMR spectra of Van-OH, respectively, corresponding to the –CH=N– and –CH=N– in Van-OH.[49,50] In short, based on the results of the FTIR, ^{1}H NMR and ^{13}C NMR spectra, it can be demonstrated that Van-OH containing C=N bonds has been successfully obtained.

Fig. 2(a) shows the FTIR spectra of the COPU sample and the four different CVPU samples. It can be seen that the peaks corresponding to the stretching vibration of the amino N–H appear at 3357 cm^{-1}, the peaks corresponding to the stretching vibration peak of the methylene C–H appear at 2924 cm^{-1} and 2844 cm^{-1}, the peaks corresponding to the stretching vibration peaks of C=O in the urethane groups appear at 1742 cm^{-1}, the peaks corresponding to the in-plane bending vibration peak of the amino N–H appear at 1525 cm^{-1}, and the peaks corresponding to the stretching vibration peaks of the C–O bond appear at 1238 cm^{-1}. In addition, no characteristic absorption peaks corresponding to the –NCO groups can be observed in all samples, indicating that all the –NCO groups were consumed during the synthesis process.[38,40] These above results demonstrate that all the samples contain the characteristic structures of PU materials.[38–43] Fig. S4 shows a partial enlargement of the FTIR spectra. By comparing the infrared spectra of the COPU and CVPU samples, it can be seen that new characteristic absorption peaks appear at 1640 cm^{-1} in

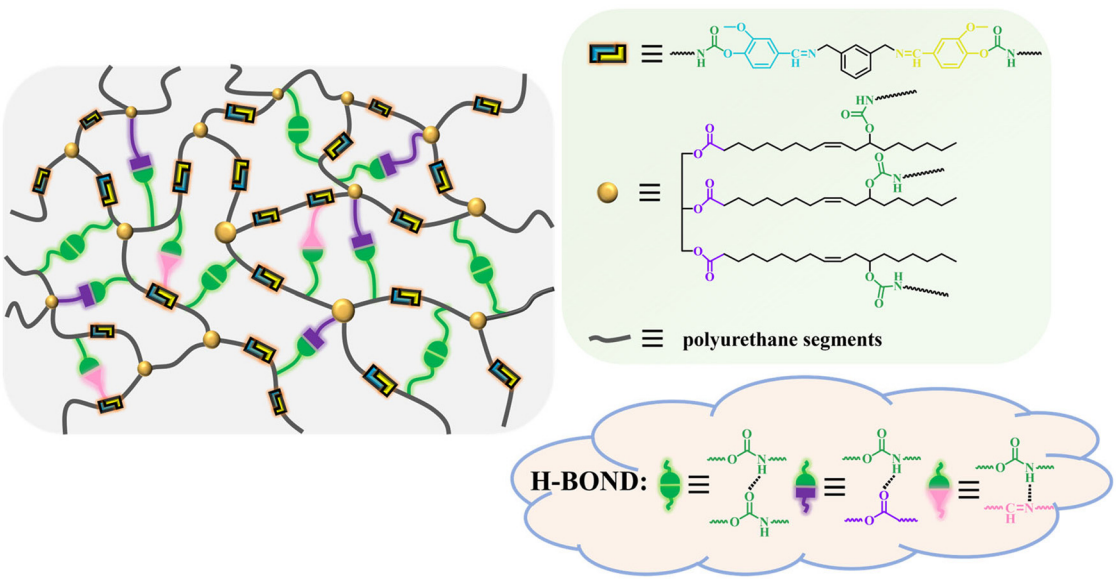

Fig. 1 Schematic diagram of the network structures of the CVPU samples.

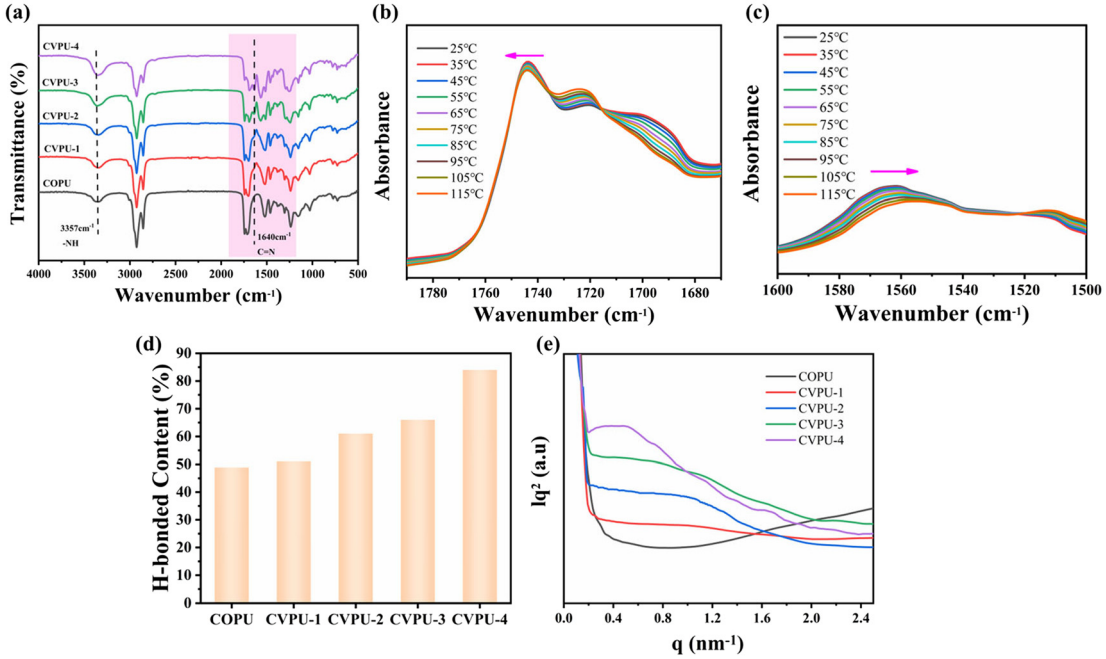

Fig. 2 (a) FTIR spectra of the COPU and CVPU samples. Variable temperature infrared spectra of (b) C═O bonds and (c) N–H bonds in the CVPU-3 sample. (d) Hydrogen bond content (H-bonded content) in the COPU and CVPU-1/2/3/4 samples. (e) SAXS patterns of the COPU and CVPU-1/2/3/4 samples.

the CVPU samples, indicating the successful introduction of the imine bonds into the system; as the Van-OH content increases, the characteristic absorption peaks of the imine bonds become more pronounced.[16] Then, based on these above results, it can be demonstrated that the COPU and CVPU samples were successfully obtained.

The C═O and N–H peaks in the CVPU-3 sample were analyzed by the variable temperature FTIR measurements, as shown in Fig. 2(b) and (c). The characteristic peaks of the C═O bonds move to higher wavenumbers, and the characteristic peaks of the N–H bonds move to lower wavenumbers with the increase of temperature, demonstrating that the hydrogen bonds gradually transformed into a free state as the temperature increased. In short, these results can demonstrate the presence of the hydrogen bonding interactions in the PU vitrimers. For PU materials, the amount of hydrogen bond affects the degree of microphase separation.[44,51] In general, the absorption peaks corresponding to the C═O stretching vibration can be back-convoluted into three sub-peaks, as shown in Fig. S5. The sub-peak at 1738 cm^{-1} with the higher wavenumber corresponds to the free C═O groups that are not involved in forming the hydrogen bonds. The sub-peak at 1720 cm^{-1} corresponds to disordered hydrogen-bonded C═O groups and at 1698 cm^{-1} to ordered hydrogen-bonded C═O groups.[38,52] Furthermore, the percentage of the hydrogen bond content for all the PU samples was calculated, as shown in Fig. 2(d). It can be seen that the hydrogen bond content in the CVPU samples gradually increases with the increase of the content of Van-OH in the hard segments. As the content of the hard segments increases, the conjugated structure of the benzene rings forms a more regular stacking structure, which reduces the distance between the hard segments, and at the same time strengthens the aggregation ability between the hard segments, making it easier to form hydrogen bonds in the hard segment intervals. That is, the higher the content of the hard segments, the higher the hydrogen bonding content, and the higher the degree of microphase separation between the hard and soft segments in the PU samples.

The microphase separation structure of the CVPU samples can be verified by the results based on the AFM measurement. As shown in Fig. S6, the bright regions represent the hard segments, and the dark regions represent the soft segments. For the COPU sample, the size of the bright regions is very small, which indicates that the degree of microphase separation is low. However, for the four CVPU samples, there are clear bright regions, indicating that the addition of the Van-OH segments can promote the microphase separation in the PU. In addition, it can also be seen that the PU samples containing the higher Van-OH content (that is, a higher content of the hard segments) have larger bright regions (a greater degree of microphase separation).

To more clearly demonstrate the microphase separation, small-angle X-ray scattering tests were further conducted on the different PU samples. In Fig. 2(e), it can be seen that the phase spacing in the PU samples gradually increases with the increase of the hard segment content, further demonstrating that the increase of the hard segment content can cause the improvement in the degree of the microphase separation.

The results based on the MD simulations can provide more structural details about the presence of hydrogen bonds and microphase separation. We analyzed the hydrogen bond formation between different groups in the two simulated systems (the simulated COPU system and simulated CVPU system). Fig. 3(a) illustrates the local conformation of the hard segments. It can be seen that there are hydrogen bonds (marked by the blue dotted lines) at both ends of the Van-OH segments. This demonstrates that the dynamic imine bonds are indeed locked in the hard microphase containing hydrogen bonds. Fig. 3(b) and (c) further display the number of hydrogen bonds formed between different groups in the two simulated systems. In the simulated CVPU systems, there exist three kinds of hydrogen bonds: the hydrogen bonds forming between the ester groups in the CSO segments and urethane groups, the hydrogen bonds forming between the urethane groups and imine groups, and the hydrogen bonds forming between the two urethane groups. In the simulated COPU systems, there exist only two kinds of hydrogen bonds: the hydrogen bonds forming between the ester groups in the CSO segments and urethane groups, and the hydrogen bonds forming between the two urethane groups. In addition, the total number of hydrogen bonds in the simulated CVPU system is apparently higher than that of the hydrogen bonds in the simulated COPU system. That is, the incorporation of the Van-OH segments can cause an increase of the hydrogen bond content, which is consistent with the above experimental results.

Furthermore, the χ_{mix} was calculated to evaluate the degree of the microphase separation based on the following equations:

$$\frac{\Delta E_{mix}}{V} = \varnothing_{SS}\left(\frac{E_{coh}}{V}\right)_{SS} + \varnothing_{HS}\left(\frac{E_{coh}}{V}\right)_{HS} - \left(\frac{E_{coh}}{V}\right)_{mix} \quad (3)$$

$$\chi_{mix} = \frac{1}{\varnothing_{SS}\varnothing_{HS}}\left(\frac{\Delta E_{mix}}{K_b T}\right) \quad (4)$$

where the subscript SS represents the soft segments, the subscript HS represents the hard segments, ΔE_{mix} represents the mixing energy, V represents the volume, the E_{coh} represents the cohesive energy, and $\varnothing_{SS}$ and $\varnothing_{HS}$ represent the volume fraction of the soft segments and the hard segments, respectively. The calculation results are listed in Table 1. The values of ΔE_{mix} and χ_{mix} in the simulated CVPU system are higher than those in the simulated COPU system, demonstrating that the microphase separation degree in the CVPU system containing the imine bonds is higher than that of the COPU system without the imine bonds. That is, after the introduction of the Van-OH segments containing the imine bonds, the degree of

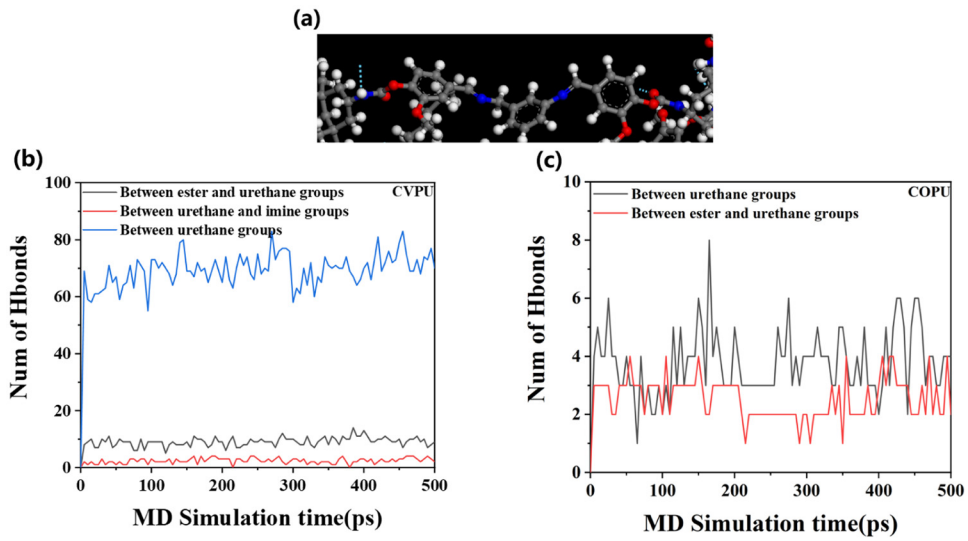

Fig. 3 (a) Snapshots of the local conformation of the hard segments. (b) The number of hydrogen bonds (Num of Hbonds) forming between different groups in the simulated CVPU system. (c) The number of hydrogen bonds forming between different groups in the simulated COPU system.

Table 1 Results of the Flory–Huggins parameters for the interaction between the hard segments and soft segments

	$\varnothing_{HH}$	$\varnothing_{HS}$	$\left(\frac{E_{coh}}{V}\right)_{SS}$	$\left(\frac{E_{coh}}{V}\right)_{HS}$	$\left(\frac{E_{coh}}{V}\right)_{mix}$	ΔE_{mix}	χ_{mix}
CVPU	0.45	0.55	2.99×10^8 J m^{-3}	4.63×10^8 J m^{-3}	2.93×10^8 J m^{-3}	56 376.42 J mol^{-1}	108.36
COPU	0.70	0.30	2.99×10^8 J m^{-3}	5.20×10^8 J m^{-3}	3.43×10^8 J m^{-3}	7100.56 J mol^{-1}	13.65

microphase separation will increase, which is consistent with the above experimental findings.

The crosslinking density of the three different PU samples (the COPU sample, CVPU-3 sample and CVPU-4 sample) is shown in Table S2. The COPU sample has the highest crosslinking density, and the CVPU-4 sample exhibits a lower crosslinking density than the CVPU-3 sample. These results demonstrate that the prepared PU samples contain the crosslinking networks. In the current experiments, the incorporation of chemical crosslinking points results from the introduction of the CSO molecules with trifunctional groups into the PU chains. For the CVPU samples, the number of CSO molecules is kept constant, and then with the gradual increase in the number of Van-OH segments, the number of chemical bonds in the PU chains is increased, leading to a decrease in the crosslinking density.

The XRD patterns of the COPU sample and the CVPU samples are shown in Fig. S7. Wide peaks can be observed at 2θ = 19°, indicating that no crystallization occurs in the soft segments of the PU samples.[53] In addition, the peak intensity of the CVPU samples is higher than that of the COPU sample, and increases with the increase of the Van-OH content. The Van-OH structure belongs to an anisotropic rigid element, and then the presence of the Van-OH structure will improve the local orders of the PU segments.[54]

Fig. 4(a) displays the curves of the tan δ of the COPU sample and CVPU samples. The temperature corresponding to the peak of the tan δ curve can be regarded as the glass transition temperature (T_g). Then, it can be seen that the value of the T_g of the COPU sample is around 10 °C; as the Van-OH content increases, the values of the T_g of the CVPU samples increase gradually (the values of the T_g of the CVPU-1 sample, CVPU-2 sample, CVPU-3 sample, and CVPU-4 sample are 30 °C, 40 °C, 52 °C, and 80 °C, respectively). This increase of the T_g can be attributed to the incorporation of the rigid Van-OH structure. It should be noted that in PU materials, soft segments should theoretically have their own T_g, but in the DMA measurements, only one T_g is observed. There are two reasons for this phenomenon. On one hand, intermolecular hydrogen bonds can be formed between the carbonyl groups in the CSO segments and the urethane NH groups, resulting in an enhancement in the interactions between the soft and hard segments. On the other hand, unlike other commonly used soft segments (such as polycarbonate glycol), CSO has a much smaller molecular weight. The above two reasons may cause the T_g peak of the soft segments to overlap with or be masked by that of the hard segments, ultimately resulting in only one T_g peak appearing in the PU materials. As shown in Fig. 4(b), at room temperature, the storage modulus (E') of the COPU sample is the smallest (3.87 MPa), followed by the E' of the CVPU-1 sample (25.38 MPa), CVPU-2 sample (163.76 MPa), and CVPU-3 sample (318.15 MPa), and the E' of the CVPU-4 sample is the largest (366.84 MPa). These results demonstrate that the addition of the rigid Van-OH segments can remarkably improve the modulus and stiffness of the PU materials.

Fig. 4(c) shows the TGA curves of the COPU sample and the different CVPU samples under a N_2 atmosphere from 25 °C to 600 °C. It can be seen that the thermal weight loss process of the COPU sample and the CVPU samples has three stages. The first stage is within the temperature range of 25 °C–310 °C, and the thermal weight loss during this stage is mainly caused by the volatilization of water and small molecules, with a relatively small proportion.[55] The second stage is in the temperature range of 310 °C–338 °C and is mainly caused by the volatilization of the hard segments.[56] The COPU sample does not contain the Van-OH segments, and thus its weight loss in the second stage is mainly caused by the thermal degradation of the IPDI segments. In contrast, the second stage of the CVPU samples is related to the degradation of Van-OH and IPDI in the hard segments. The third stage is within the temperature range from 338 °C to 470 °C with a significant proportion of weight loss, which is mainly caused by the volatilization of the soft CSO segments.[57]

Table S3 shows the thermal properties of the five PU samples. It can be seen that the values of the T_5 of the CVPU samples gradually decrease with the increase of the contents of Van-OH. The addition of the Van-OH segments reduces the covalent crosslinking density of the PU materials, and the stability of the imine bonds is relatively low. Then, the CVPU samples containing a greater number of Van-OH segments and imine bonds will have lower thermal stability. However, it should be noted that the initial decomposition temperatures of all the CVPU samples are higher than 190 °C, which is higher than the processing temperature (≤180 °C), indicating

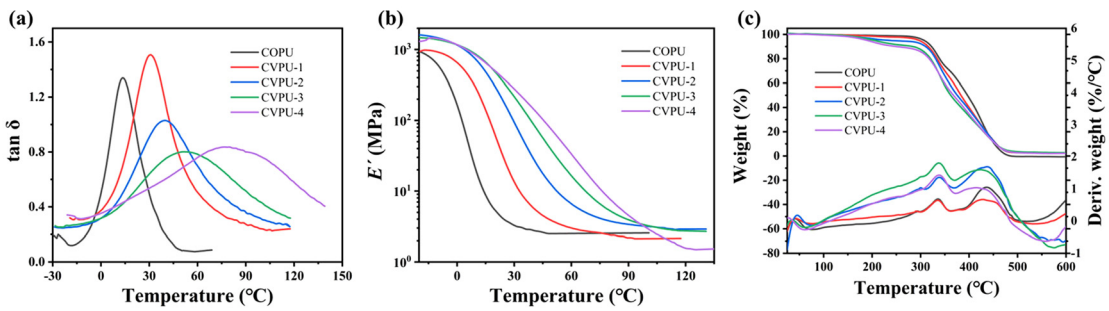

Fig. 4 (a) tan δ and (b) E' as a function of temperature for the COPU and CVPU samples. (c) TGA and DTG curves of the COPU sample and the different CVPU samples under a N_2 atmosphere from 25 °C to 600 °C.

that the CVPU samples have sufficient stability during the processing. Isothermal TGA testing was performed on the different PU samples, the results of which are shown in Fig. S8. These samples were placed at the processing temperature (180 °C) for 40 min. It can be seen that all the samples only show a slight decline in weight, indicating that the polymer structures remain basically unchanged after the hot pressing.

Then, we focused on the dynamicity of the imine bonds in the CVPU samples. Fig. 5(a) displays the curves of the stress relaxation of the five PU samples measured at 160 °C. Herein, according to the Maxwell model, the time required for the stress to relax to $1/e$ of the initial value can be treated as the relaxation time (τ).[24,58] It can be seen that the decrease rate of the stress of the COPU sample is the slowest, and the stress value does not decrease to $1/e$ of its original value during the stress relaxation experiment, indicating that no significant stress relaxation phenomenon occurs in the COPU sample, which can be attributed to the lack of the dynamic imine bonds in the COPU sample. In addition, the other four CVPU samples all exhibit significant stress relaxation, and the CVPU samples containing more dynamic covalent bonds have faster rates of stress reduction. Then, the values of τ of the four CVPU samples can be calculated, as listed in Table 2. It can be seen that the CVPU samples containing more dynamic imine bonds have lower values of τ, also suggesting that the presence of more dynamic imine bonds will promote the relaxation of polymer chain segments. The effect of temperature on the stress relaxation process was also investigated. Fig. 5(b) and Fig. S9(a–c) show the variation of the stress over time during the stress relaxation process of the CVPU-1/2/3/4 sample at different temperatures. All the samples exhibit a faster decrease in stress at higher temperatures, suggesting that an increase in temperature improves the relaxation of the PU chain segments. This can be attributed to the fact that high temperatures accelerates the rate of imine bond exchange, which leads to an increase in the relaxation rate.[24,58]

Table 2 Values of the relaxation time of the four CVPU samples

Sample	CVPU-1	CVPU-2	CVPU-3	CVPU-4
τ(s)	1217.51	417.38	344.82	20.73

Furthermore, based on the above experimental results on the relaxation time at different temperatures, the relaxation activation energy (E_a) of the CPUV-3 sample can be calculated based on the Arrhenius equation:[24]

$$\ln \tau = \ln \tau_0 + \frac{E_a}{RT} \quad (5)$$

where τ_0 is the characteristic relaxation time at infinite temperature, R is the gas constant, T is temperature, and E_a is the activation energy of the bond exchange process. Fig. 5(c) and

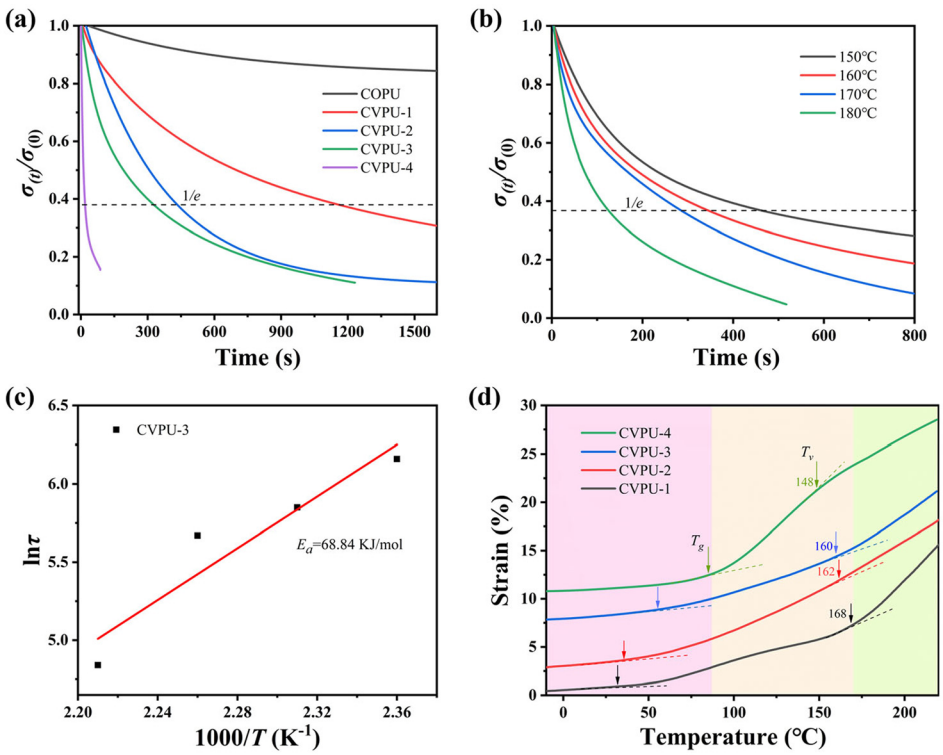

Fig. 5 (a) Changes of the relative stress ($\sigma_{(t)}/\sigma_{(0)}$) of COPU and CVPU-1/2/3/4 as a function of time at 160 °C during stress relaxation. (b) Changes of the $\sigma_{(t)}/\sigma_{(0)}$ of the CVPU-3 at different temperatures during stress relaxation. (c) ln τ as a function of 1000/T for the CPUV-3 sample (the solid line was obtained by fitting the data based on the Arrhenius equation). (d) Change of strain as a function of temperature for the CVPU-1/2/3/4 samples during the TMA testing.

Fig. S9(d) display the values of In τ as a function of 1000/T. Then, the values of E_a of the imine bond exchange reaction for the CVPU-1/2/3/4 samples were calculated by fitting the data based on the Arrhenius equation, and they are 109.25 kJ mol^{-1}, 102.43 kJ mol^{-1}, 68.84 kJ mol^{-1}, and 55.21 kJ mol^{-1}, respectively. The R^2 values corresponding to the fitting of the Arrhenius plots are listed in Table S4. It can be seen that all the R^2 values are bigger than 0.90, demonstrating that the fitting achieves a relatively satisfactory performance. It can be seen that the CVPU samples containing higher contents of imine bonds exhibit lower values of E_a. That is, the presence of the imine bonds is beneficial for enhancing the relaxation ability of the chain segments in the covalently crosslinked PU. In short, at relatively high temperatures, the imine bonds of the CVPU samples have the ability to break and reform, thus resulting in the strong relaxation ability.[59]

Topological freezing transition temperature (T_v) is a key characteristic of the vitrimers.[22–26] Above the T_v, the exchange reaction rate of the dynamic covalent bonds is fast, and thus the segments of the vitrimers have strong mobility (the corresponding vitrimer samples will have a low modulus). Below the T_v, the dynamic covalent bonds are in a frozen state due to their extremely slow exchange reaction rate, and then the vitrimers cannot undergo structural adjustments (the corresponding vitrimer samples will have a high modulus). Fig. 5(d) shows the changes of strain as a function of temperature for the four CVPU samples during the TMA testing. The values of the strain of all the four CVPU samples undergo two significant changes, corresponding to the occurrence of the glass transition (the first strain change at a relatively low temperature region) and the topological freezing transition (the second strain change at a relatively high temperature region), respectively. Then, the values of T_g and T_v can be obtained, as shown in Fig. 5(d). The values of T_g are consistent with the results obtained based on DMA testing. At the T_v, the dynamic exchange of the imine bonds is activated, allowing for a sudden change in the strain. In addition, the CVPU samples with the higher contents of imine bonds have lower T_v and thus the faster rate of network rearrangements. This result is consistent with the above results based on the stress relaxation.

Properties of PU vitrimers

The stress–strain curves of the five different PU samples are displayed in Fig. 6(a), and the values of the tensile strength, elongation at break and Young's modulus are listed in Table S5. The COPU sample exhibits the worst mechanical properties (the tensile strength, Young's modulus, elongation at break, and toughness are 1.47 MPa, 4.39 MPa, 384.74%, and 2.93 MJ m^{-3}, respectively). After adding appropriate amounts of Van-OH, the four properties of the PU samples can be dramatically improved. For instance, the tensile strength, Young's modulus, elongation at break, and toughness of the CVPU-3 sample can reach 28.43 MPa (19.34 times that of the COPU sample), 597.99 MPa (136.2 times that of the COPU sample), 400.62%, and 68.75 MJ m^{-3} (23.46 times that of the COPU sample), respectively. However, the addition of excessive Van-OH into the PU can lead to high contents of rigid structures, which will greatly improve the tensile strength and Young's modulus of the PU, but reduce the elongation at break. It can be seen that the CVPU-4 sample with the highest content of Van-OH segments exhibits the highest tensile strength (36.69 MPa; 24.9 times that of the COPU sample) and Young's modulus (1751.83 MPa; 399.05 times that of the COPU sample) but the lowest elongation at break (238.52%), respectively (its toughness of 66.64 MJ m^{-3} is slightly lower than that of the CVPU-3 sample and 22.74 times that of the COPU sample). In short, there is an optimal content of the Van-OH segments, below which the CVPU sample will exhibit both better tensile strength and elongation at break, compared with those of the COPU sample. That is, the presence of the Van-OH segments has a remarkable enhancement effect on the mechanical properties of the PU vitrimers. On one hand, the addition of the Van-OH segments can lead to an increase of the hydrogen bond number and hard phase content, which is beneficial for the improvement in the tensile strength of the PU samples. On the other hand, the addition of the Van-OH segments also leads to a decrease in the crosslinking density of the CVPU samples, which in turn increases the elongation at break. However, in the CVPU samples containing the Van-OH segments exceeding the optimal content, the presence of the rigid

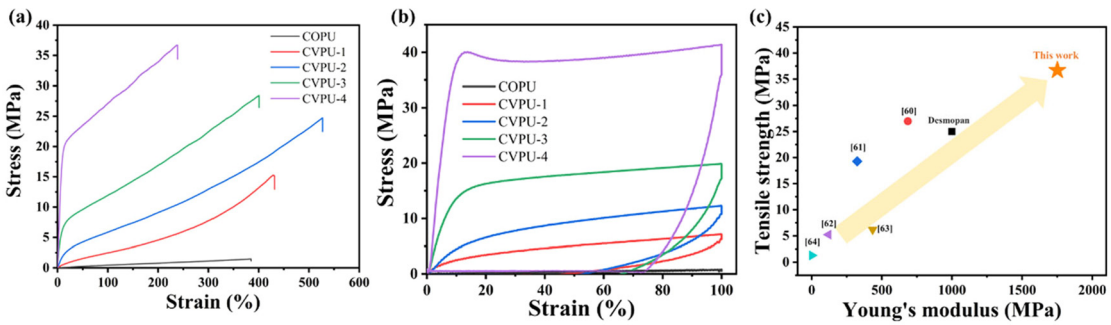

Fig. 6 (a) Stress–strain curves for the COPU sample and CVPU-1/2/3/4 samples. (b) Stress–strain curves for the COPU sample and CVPU-1/2/3/4 samples based on the cyclic tensile test. (c) Comparison of the tensile strength and Young's modulus of CVPU-4 with those of a commercialized PU material and some PU vitrimers in the relevant literature.[60–64]

Van-OH segments will lead to an increase of the network rigidity, thus causing a decrease in the elongation at break of the CVPU samples.

The stress–strain curves of the cyclic stretching experiments of the five PU samples are shown in Fig. 6(b), and the corresponding values of the hysteresis loop areas of the cyclic stress–strain curves are shown in Table S6. The size of the hysteresis loop area reflects the ability to dissipate energy in the PU samples during a loading–unloading cycle.[17,32,42] The hysteresis loop area gradually increases with the increase of the Van-OH content. That is, in the PU vitrimers containing more Van-OH segments, there are more hard segments (stronger degree of microphase separation) and more hydrogen bonds. In this way, more intermolecular interactions will be disrupted during the stretching process, resulting in a larger hysteresis loop.

We compared the tensile strength and Young's modulus of CVPU-4 with those of a commercialized PU material (Desmopan) and some PU vitrimers in the relevant literature,[60–64] as shown in Fig. 6(c). The tensile strength and modulus of CVPU-4 are apparently higher than those of the commercialized PU material (Desmopan) and the reported PU vitrimers with dynamic bonds.[60–64] This indicates that the PU vitrimers prepared in the current work exhibit obvious advantages in terms of mechanical strength.

Fig. S10 depicts the results of the water contact angle test. It can be seen that the values of the contact angle of the COPU sample and the CVPU samples are all less than 90°, indicating that these PU samples have a certain degree of hydrophilicity, which is conducive to improving their adhesive strength to the surface of polar substrates.

It should be noted that the CVPU samples have good resistance to organic solvents. The CVPU-3 samples were soaked in different organic solvents (ethanol, tetrahydrofuran (THF), acetone, DMF, and chloroform) at room temperature for 7 d, as shown in Fig. S11. The CVPU-3 samples only swell in the solvents and do not dissolve, confirming that the CVPU-3 sample has good resistance to organic solvents.

The adhesion performance of the CVPU-3 sample was also tested. As shown in Fig. 7(a), the two horizontally placed steel plates bonded by the CVPU-3 sample can support an object

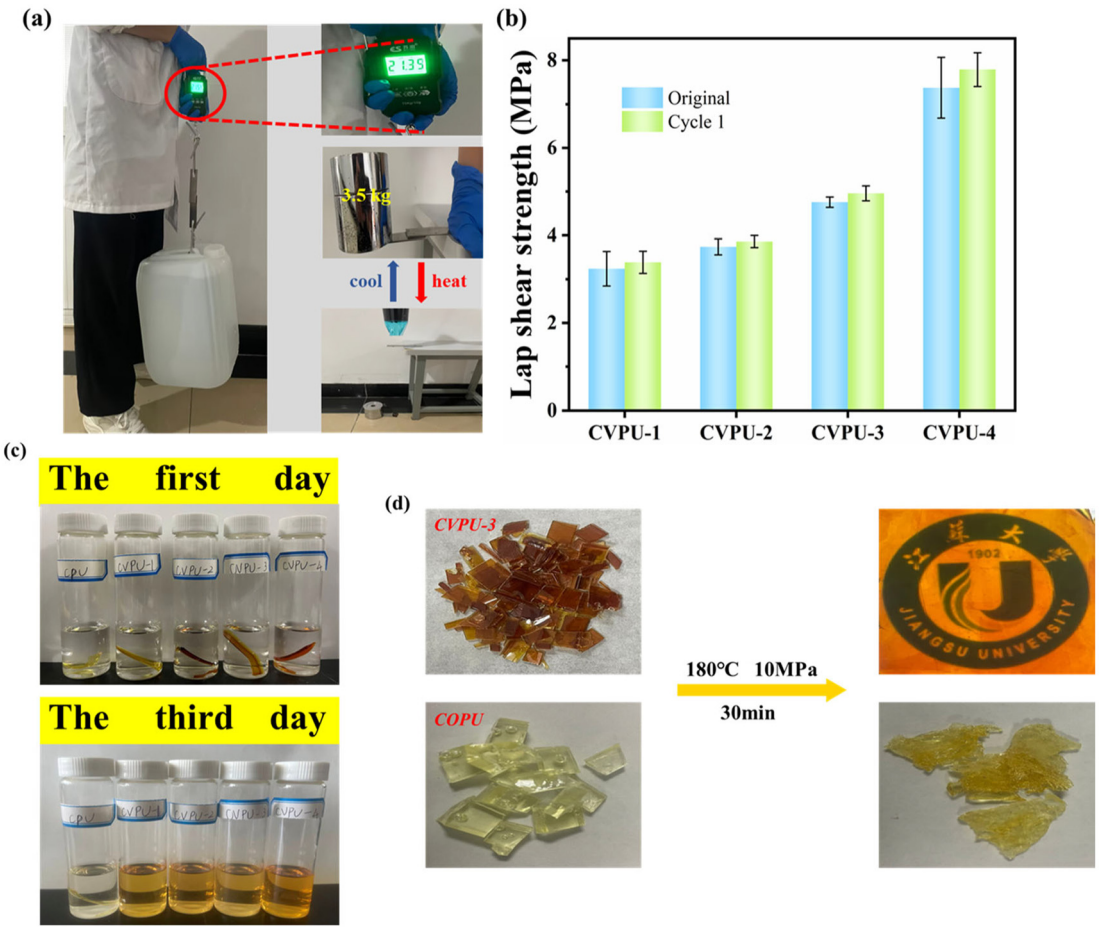

Fig. 7 (a) A pair of steel plates bonded by the CVPU-3 sample can be used to lift a weight of 20 kg; or when two steel plates are placed horizontally, they can support a weight of 3.5 kg, but the two steel plates become detached when heated. (b) Lap shear strength of the original CVPU films and the re-bonded CVPU films (the cycle 1). (c) Photographs of the COPU and different CVPU samples soaked in the mixed solvent of HCl and H_2O for 3 days. (d) Photographs of the COPU and CVPU-3 samples before and after the remolding process.

weighing 3.5 kg. In addition, it can also be seen that the two steel plates bonded by the CVPU-3 sample with a bonding area of 3.125 cm^2 can lift a water bucket filled with water weighing approximately 20 kg. These above results demonstrate that the CVPU-3 sample has high adhesive strength. Fig. 7(b) displays the lap shear strength of the different CVPU samples. It can be seen that the CVPU samples containing more Van-OH segments exhibit higher lap shear strength. That is, the incorporation of the imine bonds is beneficial for the improvement in the adhesive strength of PU. In addition, the CVPU films have an effective re-bonding ability. It can be seen in Fig. 7(b) that all the CVPU films re-bonded with the steel plates exhibit similar values of adhesive strength to the original CVPU films.

Then, we focused on the recyclability of the PU materials. In general, the imine bonds can undergo hydrolysis reaction under acidic conditions, leading to the destruction of the crosslinked structure.[65] In order to investigate the recyclability of the CVPU samples under acidic conditions, the five PU samples were soaked in a 0.1 mol L^{-1} HCl aqueous solution at room temperature, as shown in Fig. 7(c). After soaking these PU samples for 3 d, the CVPU samples containing the imine bonds show excellent solubility (there are no insoluble residues inside the corresponding tubes). However, the COPU sample without imine bonds in the tube does not significantly dissolve. In short, the presence of imine bonds can endow the crosslinked PU materials with recyclability.

The reprocessability of the CVPU samples was further tested. The samples of small pieces of the PU samples were remolded at 180 °C and 10 MPa for 20 min to assess the reprocessability. Fig. 7(d) shows the appearance of the two PU samples (the COPU sample and CVPU-3 sample) obtained through the remolding. It can be seen that the COPU sample of small pieces cannot be reprocessed into a complete sheet, which is attributed to the presence of the permanent covalent crosslinking structure in the COPU sample. However, the CVPU-3 sample of small pieces can be reprocessed into a complete and transparent sheet, as shown in Fig. 7(d).

The FTIR, tensile and DMA tests were carried out on the different remolded CVPU samples to evaluate the structural and performance recovery of the samples. The FTIR spectra of the remolded CVPU samples were basically the same as those of the original samples (Fig. 8(a)), indicating that there were no significant changes in the chemical structures of the PU samples. The DMA and tensile tests show that the thermal and mechanical properties of the remolded samples can be largely recovered under the same test conditions (Fig. 8(b–d)). However, the T_g and tensile strength of the remolded samples are slightly higher, and the elongation at break is slightly lower compared with those of the original samples. During the remodeling process, the materials undergo a local reorganization, resulting in more tightly packed molecular chains and enhanced intermolecular hydrogen bonding interactions, which will result in an increase in both the T_g and tensile

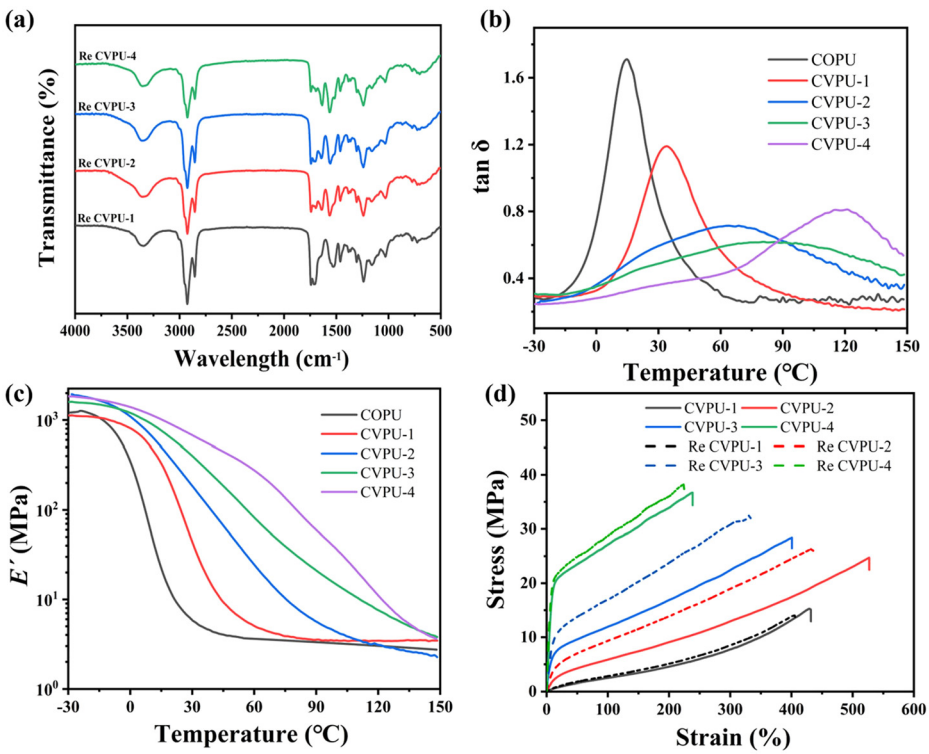

Fig. 8 (a) FTIR spectra of the remolded CVPU-1/2/3/4 samples. (b) tan δ and (c) E' as a function of temperature for the remolded CVPU-1/2/3/4 samples. (d) Stress–strain curves of the original CVPU samples and the remolded (Re) CVPU samples.

strength, while simultaneously causing a reduction in the elongation at break. In short, the CVPU samples with the dynamic imine bonds can still maintain excellent mechanical properties after remolding, that is, they have excellent reprocessability.

It should be noted that the dynamicity of dynamic covalent bonds will influence the material properties. For instance, if boronate ester bonds with stronger dynamicity are introduced into the PU chains instead of imine bonds, the mechanical properties of PU may be weaker, as the boronate ester bonds are more susceptible to breaking during stretching. However, the PU containing the boronate ester bonds will have better self-healing ability, since the boronate ester bonds are more likely to re-form after being broken. In future work, we will further systematically study the influence of introducing dynamic covalent bonds with different dynamicity on the performance of PU materials.

Conclusions

We prepared PU vitrimers containing covalent crosslinking networks, dynamic imine bond networks and hydrogen bond networks, which have high mechanical properties (tensile strength and modulus), excellent recyclability and reprocessability. These three special network structures (the covalent crosslinking network, hydrogen bond network and dynamic imine bond network) and two structural features (the microphase separation structure and rigid structures containing benzene) of the dynamic covalent bonds can all contribute to the improvements in polymer properties. The presence of the covalent crosslinking network is beneficial for improving the thermal stability and resilience of the PU materials. The hydrogen bonds have strong dynamicity, and their presence will cause much energy dissipation during stretching, which is beneficial for improving the toughness of the PU materials. Introducing the dynamic imine bonds can endow the crosslinked PU materials with recyclability. However, a disadvantage of polymers containing dynamic covalent bonds is that the low bond energy and stability of dynamic bonds will lead to a decrease in the mechanical properties of the polymers in practical use, which is not conducive to their practical applications. In the work of Dong's group,[44] the dynamic disulfide bonds were introduced into the hard segments, and then the weak disulfide bonds could be protected from breakage during stretching, thereby improving the strength of the material. In our current work, since the dynamic imine bonds were incorporated into the hard domains containing intermolecular hydrogen bonds, they had higher stability, which is beneficial for the enhancement of the mechanical properties of the PU materials. Rigid benzene rings were attached to both ends of the imine bonds, which is also conducive to improving the mechanical properties of the PU vitrimers. In addition, unlike the work of Dong's group, the component introduced in this study contains dynamic imine bonds along with some groups capable of participating in hydrogen bond formation. Combining experimental and simulation results, we found that the incorporation of this component can cause the increase of the hydrogen bond content and promote a more pronounced microphase separation. These results provide new ideas for the design of the PU materials with high mechanical properties, high recyclability and high reprocessability.

Author contributions

X. Du synthesized and characterized the polymer materials and wrote the first draft. L. Shuai carried out the simulation work. S. Wang participated in the synthesis and preparation of the polymer materials. H. Wu participated in the characterization of the material structure. J. Li participated in the material reprocessing experiment. J. Wen participated in the computer simulation work. M. Zhu and J. Hu participated in the design and guidance of the experimental work. Y. Nie provided guidance in the experimental work and revised the manuscript.

Conflicts of interest

The authors declare no conflict of interest.

Data availability

Synthesis route of the Van-OH, the COPU and the CVPU; Snapshots for the simulated CVPU system and the simulated COPU system; FTIR spectrum, ^{1}H NMR spectrum and ^{13}C NMR spectrum of the Van-OH; Localized magnification of FTIR spectra; AFM images; XRD patterns; Isothermal TGA curves; Stress relaxation curves; Water contact angle; Photos of samples soaked in solvents; Formulation of different PU samples; Crosslinking density; Thermal stability data; The R^2 values; Mechanical properties; Hysteresis loop areas. Data will be made available on request. Supplementary information is available. See DOI: **https://doi.org/10.1039/d5py00728c**.

Acknowledgements

This work was financially supported by National Natural Science Foundation of China (No. 52173020) and Qing Lan Project of Jiangsu Province, China ([2022]29).

References

1 T. P. Haider, C. Völker, J. Kramm, K. Landfester and F. R. Wurm, *Angew. Chem., Int. Ed.*, 2019, **58**, 50–62.
2 C. Zhang, H. Cui, Y. Han, F. Yu and X. Shi, *Food Chem.*, 2018, **240**, 893–897.

3 Y. Lu, Y. Zhang and K. Zhang, *Chem. Eng. J.*, 2022, **448**, 137670.
4 K. L. Law and R. Narayan, *Nat. Rev. Mater.*, 2022, **7**, 104–116.
5 X. Jiang, B. Zhu and M. Zhu, *Green Chem.*, 2023, **25**, 6971–7025.
6 I. A. Lakhiar, H. Yan, J. Zhang, G. Wang, S. Deng, R. Bao, C. Zhang, T. N. Syed, B. Wang, R. Zhou and X. Wang, *Agronomy*, 2024, **14**, 548.
7 Y. Liu, Z. Yu, B. Wang, P. Li, J. Zhu and S. Ma, *Green Chem.*, 2022, **24**, 5691–5708.
8 W. Post, A. Susa, R. Blaauw, K. Molenveld and R. J. Knoop, *Polym. Rev.*, 2020, **60**, 359–388.
9 J. M. Winne, L. Leibler and F. E. Du Prez, *Polym. Chem.*, 2019, **10**, 6091–6108.
10 S. Yu, F. Li, S. Fang, X. Yin, S. Wu, Z. Tang, L. Zhang and B. Guo, *Macromolecules*, 2022, **55**, 3236–3248.
11 J. Yu, H. Yang, H. Ji, X. Zhang, R. Wang, S. Zhao, R. Wang and L. Zhang, *ACS Omega*, 2023, **8**, 32146–32158.
12 P. T. Corbett, J. Leclaire, L. Vial, K. R. West, J. L. Wietor, J. K. Sanders and S. Otto, *Chem. Rev.*, 2006, **106**, 3652–3711.
13 J. M. Lehn and A. V. Eliseev, *Science*, 2001, **291**, 2331–2332.
14 J. M. Lehn, *Chem. Soc. Rev.*, 2007, **36**, 151–160.
15 A. Chao, I. Negulescu and D. Zhang, *Macromolecules*, 2016, **49**, 6277–6284.
16 F. Song, Z. Li, P. Jia, M. Zhang, C. Bo, G. Feng, L. Hu and Y. Zhou, *J. Mater. Chem. A*, 2019, **7**, 13400–13410.
17 J. Huang, Z. Gong and Y. Chen, *Polymer*, 2022, **242**, 124569.
18 H. Wang, B. Jin, H. Wu, C. Wang and J. Wu, *CCS Chem.*, 2025, **7**, 1534–1542.
19 S. Terryn, J. Brancart, E. Roels, R. Verhelle, A. Safaei, A. Cuvellier, B. Vanderborght and G. Van Assche, *Macromolecules*, 2022, **55**, 5497–5513.
20 N. Zheng, Y. Xu, Q. Zhao and T. Xie, *Chem. Rev.*, 2021, **121**, 1716–1745.
21 H. Xu, Y. Zhang, H. Wang and J. R. Wu, *Chin. J. Polym. Sci.*, 2023, **41**, 926–932.
22 D. Montarnal, M. Capelot, F. Tournilhac and L. Leibler, *Science*, 2011, **334**, 965–968.
23 J. Xia, J. A. Kalow and M. O. de la Cruz, *Macromolecules*, 2023, **56**, 8080–8093.
24 Y. Tao, X. Liang, J. Zhang, I. M. Lei and J. Liu, *J. Polym. Sci.*, 2023, **61**, 2233–2253.
25 J. Li, J. Sun, K. Lv, Y. Ji, X. Huang, Y. Bai, J. Wang, J. Jin, S. Shi and J. Liu, *J. Mol. Liq.*, 2022, **367**, 120513.
26 P. Tan, X. Zhao, Z. Zhang, W. Wei, J. Zhou, Y. Shao, X. Ma, S. Wei, Z. Gao and S. Han, *ACS Appl. Polym. Mater.*, 2024, **6**, 8977–8988.
27 S. Ji, W. Cao, Y. Yu and H. Xu, *Adv. Mater.*, 2015, **27**, 7740–7745.
28 D. M. Xie, D. X. Lu, X. L. Zhao, Y. D. Li and J. B. Zeng, *Ind. Crops Prod.*, 2021, **174**, 114198.
29 Y. Peng, S. Gu, Q. Wu, Z. Xie and J. Wu, *Acc. Mater. Res.*, 2023, **4**, 323–333.
30 W. Li, H. Wu, Y. Huang, Y. Yao, Y. Hou, Q. Teng, M. Cai and J. Wu, *Angew. Chem., Int. Ed.*, 2024, **136**, e202408250.
31 X. Liu and J. Sun, *Aggregate*, 2021, **2**, e109.
32 W. Zheng, C. Zhang, Y. Han, W. Wang and Z. Li, *Small*, 2024, **20**, 2402124.
33 J. Li, X. Du, A. Zhang, J. Wen, L. Shuai, S. Li, M. Zhu and Y. Nie, *Mater. Chem. Front.*, 2024, **8**, 3828–3858.
34 Yu. Zhou, J. Wen and Y. Nie, *Macromolecules*, 2024, **57**, 3258–3270.
35 Z. H. Zhao, S. Y. Chen, P. C. Zhao, W. L. Luo, Y. L. Luo, J. L. Zuo and C. H. Li, *Angew. Chem.*, 2024, **136**, e202400758.
36 X. Huang, A. Zhang, Q. Tan, K. Gou, Y. Chen, Y. Nie and G. Weng, *Macromolecules*, 2024, **57**, 963–975.
37 Q. L. Tan, K. Gou, J. Z. Tang, M. H. Wei, C. Wang, Y. J. Nie and G. S. Weng, *Chin. J. Polym. Sci.*, 2024, **42**, 1449–1458.
38 A. Zhang, Q. Huang, X. Du, Y. Wang, J. Yang, S. Li, M. Zhu and Y. Nie, *Polym. Chem.*, 2024, **15**, 384–396.
39 X. Du, Q. Huang, Y. Zhou, H. Wu, A. Zhang, Y. Wang, J. Yang, S. Li and Y. Nie, *Surf. Interfaces*, 2024, **55**, 105451.
40 J. Wen, G. Xu, Z. Liang, S. Li, Y. Wang, J. Yang and Y. Nie, *Phys. Chem. Chem. Phys.*, 2023, **25**, 28162.
41 Z. Liang, D. Huang, L. Zhao, Y. Nie, Z. Zhou, T. Hao and S. Li, *J. Inorg. Organomet. Polym. Mater.*, 2021, **31**, 683–694.
42 G. Xu, Z. Liang, Q. Huang, Y. Wang, J. Yang and Y. Nie, *Prog. Org. Coat.*, 2023, **175**, 107391.
43 Q. Huang, Y. Liu, S. Li, M. Zhu, T. Hao, Z. Zhou and Y. Nie, *Polymer*, 2022, **246**, 124768.
44 Y. Lai, X. Kuang, P. Zhu, M. Huang, X. Dong and D. Wang, *Adv. Mater.*, 2018, **30**, 1802556.
45 T. Li, Z. Xie, J. Xu, Y. Weng and B. H. Guo, *Eur. Polym. J.*, 2018, **107**, 249–257.
46 M. M. Coleman, K. H. Lee, D. J. Skrovanek and P. C. Painter, *Macromolecules*, 1986, **19**, 2149–2157.
47 H. Sun, P. Ren and J. R. Fried, *Comput. Theor. Polym. Sci.*, 1998, **8**, 229–246.
48 J. Lichtenberger, S. C. Hargrove-Leak and M. D. Amiridis, *J. Catal.*, 2006, **238**, 165–176.
49 Y. Fuentes-Martínez, C. Godoy-Alcántar, F. Medrano and A. Dikiy, *J. Phys. Org. Chem.*, 2012, **25**, 1395–1403.
50 N. Popp, T. Homburg, N. Stock and J. Senker, *J. Mater. Chem. A*, 2015, **3**, 18492–18504.
51 C. Tao, Z. Luo, J. Bao, Q. Cheng, Y. Huang and G. Xu, *J. Mater. Sci.*, 2018, **53**, 8639–8652.
52 X. Song, M. Yu, H. Niu, Y. Zhu, K. Zhao, C. Zhou, L. Liu and G. Wu, *Eur. Polym. J.*, 2023, **200**, 112525.
53 L. H. Chan-Chan, R. Solis-Correa, R. F. Vargas-Coronado, J. M. Cervantes-Uc, J. V. Cauich-Rodríguez, P. Quintana and P. Bartolo-Pérez, *Acta Biomater.*, 2010, **6**, 2035–2044.
54 Z. Kong, W. B. Ying, H. Hu, K. Wang, C. Chen, Y. Tian, F. Li and R. Zhang, *Polymer*, 2020, **210**, 123012.
55 M. Shi, J. Yang and X. Wang, *J. Polym. Res.*, 2021, **28**, 351.
56 W. Liu, C. Fang, S. Wang, J. Huang and X. Qiu, *Macromolecules*, 2019, **52**, 6474–6484.
57 X. Zhu, W. Zhang, G. Lu, H. Zhao and L. Wang, *ACS Nano*, 2022, **16**, 16724–16735.

58 X. Kuang, G. Liu, X. Dong and D. Wang, *Mater. Chem. Front.*, 2017, **1**, 111–118.
59 S. Wang, S. Ma, Q. Li, W. Yuan, B. Wang and J. Zhu, *Macromolecules*, 2018, **51**, 8001–8012.
60 D. M. Xie, D. X. Lu, X. L. Zhao, Y. D. Li and J. B. Zeng, *Ind. Crops Prod.*, 2021, **174**, 114198.
61 C. Zhang, H. Liang, D. Liang, Z. Lin, Q. Chen, P. Feng and Q. Wang, *Angew. Chem., Int. Ed.*, 2021, **60**, 4289–4299.
62 L. Du, Z. Liu and Q. Wang, *Eur. Polym. J.*, 2023, **182**, 111732.
63 B. Zheng, T. Liu, J. Liu, Y. Cui, R. Ou, C. Guo, Z. Liu and Q. Wang, *Composites, Part B*, 2023, **257**, 110697.
64 J. Deng, X. Kuang, R. Liu, W. Ding, A. C. Wang, Y. C. Lai, K. Dong, Z. Wen, Y. Wang, L. Wang, H. J. Qi, T. Zhang and Z. L. Wang, *Adv. Mater.*, 2018, **30**, 1705918.
65 M. E. Belowich and J. F. Stoddart, *Chem. Soc. Rev.*, 2012, **41**, 2003–2024.